IOP Publishing Plasma Sources Science and Technology
Plasma Sources Sci. Technol. **33** (2024) 085001 (14pp) https://doi.org/10.1088/1361-6595/ad5eb9

Hysteresis in radio frequency capacitively coupled CF_4 plasmas

Xiao-Kun Wang[1,2], Ihor Korolov[2], Sebastian Wilczek[2,5], Ranna Masheyeva[3,4], Yong-Xin Liu[1,*], Yuan-Hong Song[1], Peter Hartmann[3], Zoltán Donkó[3] and Julian Schulze[2]

[1] Key Laboratory of Materials Modification by Laser, Ion, and Electron Beams (Ministry of Education), School of Physics, Dalian University of Technology, Dalian 116024, People's Republic of China
[2] Chair of Applied Electrodynamics and Plasma Technology, Department of Electrical Engineering and Information Sciences, Ruhr-University Bochum, 44801 Bochum, Germany
[3] Institute for Solid State Physics and Optics, HUN-REN Wigner Research Centre for Physics, 1121 Budapest, Hungary
[4] Department of General Physics, Satbayev University, 050013 Almaty, Kazakhstan
[5] TH Georg Agricola University, 44787 Bochum, Germany

E-mail: yxliu129@dlut.edu.cn

Received 16 April 2024, revised 11 June 2024
Accepted for publication 3 July 2024
Published 5 August 2024

Abstract

Based on experiments and simulations, various plasma parameters are found to undergo a hysteresis as a function of the driving voltage amplitude in capacitively coupled CF_4 discharges. Phase Resolved Optical Emission Spectroscopy reveals that the discharge operates in a hybrid combination of the drift-ambipolar and α-mode at low voltage. In this mode, the electric field and mean electron energy are high in the electronegative plasma bulk region. As the cross section for electron attachment is appreciable only at high electron energies, this mode results in strong negative ion production and keeps the electron density low as well as the mode of plasma operation stable, when the voltage is increased moderately. Increasing the driving voltage amplitude further ultimately induces a mode transition into a pure α-mode, once the electron density increases strongly. Decreasing the voltage again results in a reverse mode transition at a lower voltage compared to the previous mode transition, because the electron density is now initially high in the bulk and, thus, the bulk electric field and mean electron energy are low resulting in inefficient generation of negative ions via electron attachment. This keeps the electron density high even at lower driving voltages. This effect leads to the emergence of two steady states of plasma operation within a certain voltage range. The different electron energy distribution functions in these two states result in markedly different generation and density profiles of F atoms, with higher values occurring in the increasing voltage branch of the hysteresis. The ion flux and mean energy at the electrodes also differ. The voltage range, where the hysteresis occurs, is affected by the ion induced secondary electron coefficient (γ). A larger value of γ results in a shift of the hysteresis voltage range towards lower values.

Keywords: hysteresis, capacitively coupled CF_4 plasma, particle in cell simulation, experimental diagnostics

* Author to whom any correspondence should be addressed.

1. Introduction

Radio frequency (RF) capacitively coupled plasmas generated in electronegative gases, such as CF_4, SF_6, and O_2, have been widely used in the semiconductor industry for plasma etching, plasma enhanced chemical vapor deposition and plasma enhanced atomic layer deposition due to their unique properties and capabilities [1–3]. In these applications, the generation and control of the fluxes and energies of reactive atomic/molecular particles and positive ions at the electrodes have significant impacts on the plasma processes. In deposition processes [4], the plasma is usually operated at high pressure to realize low ion energies, high plasma densities and low electron temperatures, while for etching [5, 6], low pressure conditions are preferred to realize strong ion anisotropy. To attain high economic efficiency and enhance market competitiveness, a stable plasma state is crucial for ensuring repeatability and a high product yield. Plasma process development requires adjusting external control parameters, leading to changes in the discharge operation mode and plasma parameters. Therefore, understanding the variations of the plasma state and the underlying physical mechanisms in response to changes of such external control parameters is necessary.

Depending on the choice of discharge conditions such plasmas can be operated in different electron power absorption modes that strongly affect the formation of process relevant plasma parameters. In addition to the common α-mode [7–9] and the γ-mode [8, 10–13], there are drift-ambipolar (DA) [14, 15] as well as the striation mode [16] in electronegative discharges. In the α-mode, ionization primarily occurs on the bulk side of the expanding sheath edge at both electrodes. As the sheath expands, electrons acquire energy and are accelerated away from the electrodes by ambipolar heating to cause strong ionization [17]. In the γ-mode, ionization is predominantly concentrated within the sheaths. Secondary electrons emitted from the electrodes due to the bombardment of ions or neutrals as well as their collisional multiplication inside the sheaths play an important role for the ionization [8, 13, 18]. These electrons are accelerated towards the bulk by the strong electric field in the sheaths, leading to intense ionization at the maximum sheath expansion phase. Often, the α-mode occurs at low pressure and low voltage, while the γ-mode is induced at high pressure and high voltage. At high pressure, due to the efficient collisional multiplication of secondary electrons in the sheaths, the electron density in the γ-mode is usually higher than in the α-mode. By increasing the voltage and/or pressure, the α- to γ-mode transition can be induced [8].

In electronegative plasmas, a low electron density and a high electric field in the plasma bulk are the main characteristics in the DA mode [14, 19]. Negative ions are confined within the plasma bulk region. To ensure quasineutrality, an electropositive region forms at the sheath boundary, leading to local peaks in electron density. Strong drift and ambipolar electric fields in the plasma bulk and at the sheath edges are induced by the low conductivity and these local maxima of the electron density at the sheath edges. Thereby, high ionization occurs in the bulk and at the collapsing sheath edge at the times of high current within each RF period. In CF_4 plasmas, a mode transition from the DA- to the γ- or α-mode can be induced by increasing the driving voltage amplitude [10, 20].

In high electronegativity ion-ion plasmas, the striation mode can occur because of the response of ions to the electric field. In this striation mode, the ion densities exhibit 'comb-like' axial profiles and the electron density and energy are modulated by the modulated electric field in the bulk region. A mode transition from the DA- to the striation mode can be induced by increasing the pressure and/or decreasing the driving voltage amplitude [21, 22]. A transition between different discharge modes inevitably leads to a sudden change in plasma parameters, which may affect the stability and performance of plasma processes.

Related to the α–γ mode transition, hysteresis effects have been observed experimentally in SiH_4 discharges [23]: different SiH emission profiles have been obtained at the same pressure and the same voltage. This study has found that once the γ-mode is established by increasing the driving voltage amplitude, it can be maintained even at lower voltage amplitudes, when the voltage is decreased again, i.e. the reverse transition from the γ- to the α-mode occurs at a lower voltage than the critical voltage of the α- to γ-mode transition. Similar hysteresis phenomena have been found in capacitively coupled radio-frequency discharges operated in methane [24]. By increasing and decreasing the current, two different steady-states were obtained at certain discharge conditions. Detailed explanations of these effects were not provided, but the conclusion was drawn that the hysteresis might be a general property of high frequency discharges that can be operated in two different modes. However, hysteresis effects during the transition of discharge modes other than the α- and γ- modes have not been reported so far to our best knowledge.

Additional studies where hysteresis effects were identified include [25], where a hysteresis induced by varying the electrode gap length was observed in an argon discharge, and [26] where a hysteresis of the measured plasma emission intensity and the computed electron-impact excitation rate was reported in dual-frequency capacitively coupled CF_4 plasmas operating in the striation mode and driven by 8 MHz and 40 MHz. In this latter study, the number of striations was found to be different when increasing and decreasing the high frequency voltage amplitude, which depends on the 'prehistory' of the discharge system.

In this work, a new type of hysteresis in capacitively coupled CF_4 discharges is observed between the α- and DA-operation modes which is understood in detail based on experimental and computational results. The transition is controlled by the driving voltage amplitude. The consequences of the hysteresis effect on process relevant plasma parameters such as radical densities, ion fluxes and energies are revealed.

This paper is structured in the following way: in section 2, the experimental setup and all diagnostic methods are introduced and the PIC/MCC code used in the numerical studies is briefly described. The results are presented in section 3. Finally, conclusions are drawn in section 4.

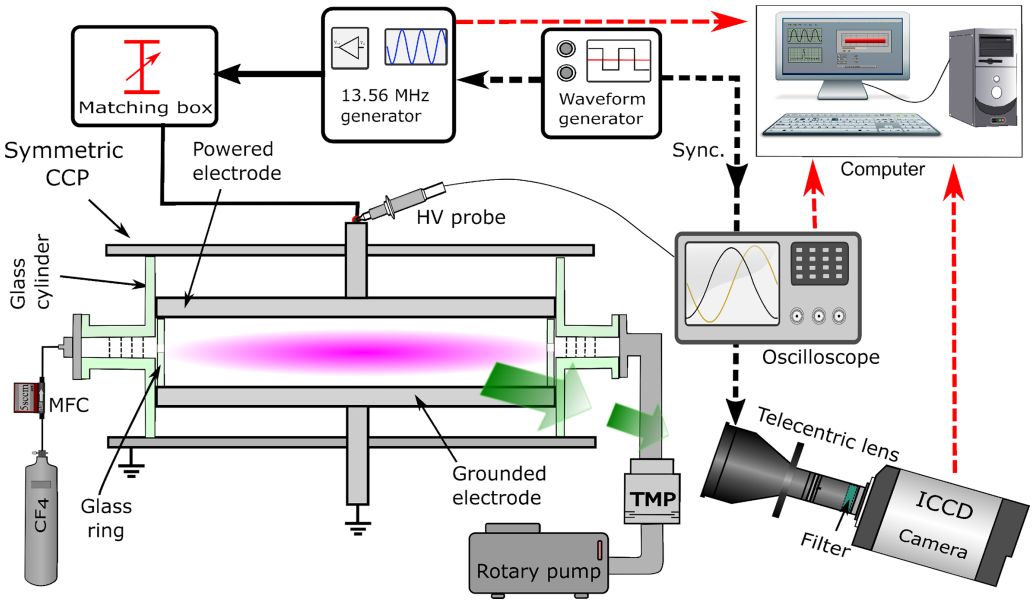

Figure 1. Sketch of the experimental setup with diagnostics.

2. Experiment and simulation methods

2.1. Experimental setup

A schematic of the experimental setup equipped with the diagnostic systems is displayed in figure 1. The discharge is generated between two equal-area stainless steel electrodes (119 mm diameter) separated by a gap of $L = 2.5$ cm inside a cylindrical borosilicate glass reactor with an inner diameter of 120 mm. Each electrode is connected to its adjacent reactor lid via a copper rod, which holds the electrode in position and establishes an electrical connection to the respective lid. The upper electrode is driven by a harmonic RF voltage waveform with a frequency of 13.56 MHz provided by an RF generator (Comet cito Plus 136) followed by a matching box. A two-channel arbitrary waveform generator (Keysight 33600A Series) is used to synchronize an ICCD camera (4 Quik E, Stanford Computer Optics) with the RF generator. The ICCD camera is triggered by a signal with a frequency of 135.6 kHz, which is phase-locked to the plasma driving voltage waveform. The voltage drop across the discharge is measured at the powered electrode by a high voltage probe (Testec TT-HVP 2739) connected to an oscilloscope (Pico Technology PicoScope 6404D). The bottom electrode is grounded.

CF_4 gas with a purity grade of 5.0 is introduced to the chamber via a mass flow controller (MCE-10SCCM-D-DB, Alicat) through a side flange of the glass cylinder. The system is pumped from the opposite side flange by a turbo molecular pump (TMP, Leybold TURBOVAC 151 C) and a rotary pump (Leybold TRIVAC D 2.5 E). Prior to the experiments, the system is pumped to a base pressure of 5×10^{-4} Pa. In this work, the pressure was kept at 20 Pa by adjusting a gate valve with a fixed gas flow rate of 5 sccm. The gas pressure is monitored by a capacitive pressure gauge (CMR 364 110 Pa, Pfeiffer, not shown in figure 1). To protect the glass wall of the chamber from deposition from the CF_4 plasma, a cylindrical glass ring with a thickness of 2 mm, an outer diameter of 100 mm, and a height equal to the electrode gap is placed between the electrodes. This part has several 5-mm-diameter holes at the positions of the ports of the chamber to ensure unobstructed gas flow through the cell. In case of eventual contamination, the glass ring can be replaced to ensure a proper transparency of the system for optical measurements. It is worth noting that in the course of the experiment we found that the plasma did not noticeably contaminate the glass side wall so that the intensity of the plasma emission was not affected by any such coatings. To maintain a consistent experimental environment, the glass ring was not replaced during the measurement in this study.

Phase resolved optical emission spectroscopy (PROES) is utilized to measure the spatio-temporally resolved excitation dynamics of energetic electrons within the RF period at different voltage amplitudes within the voltage range of hysteresis. During the measurements, the plasma is ignited at a low voltage and then the voltage is gradually increased to the desired values. In the voltage decreasing branch, the voltage is gradually decreased to the desired values from a high initial value without any voltage jumps. The fast-gated ICCD camera (mentioned above) is equipped with a telecentric lens (MVTC23013, Thorlabs) pointed at the center of the reactor chamber. The spatial resolution of the system is approximately 6 pixels per mm. A camera gate width of 2 ns is used. The camera gate is scanned through the RF period by adjusting the triggering time of the camera with respect to the applied voltage waveform by an internal camera delay generator. In the experiment, we monitor the plasma emission at a wavelength of 703.7 nm originating from the F I ($3p\ ^2P^0_{3/2} \rightarrow 3\ s\ ^2P_{3/2}$) transition with an effective lifetime of the upper level of 17.3 ns [27, 28]. The wavelength selectivity is ensured by an optical filter with a central wavelength of 704.46 nm and a full-width half maximum of 6 nm that is installed inside the telecentric length. The filter has around 75% transmission at 703.7 nm.

The spatio-temporally resolved electron impact excitation rate from the ground state into the upper level of the observed transition is calculated from the measured emission data using a collisional radiative model described in [29]. The threshold energy of this electron impact excitation is 14.75 eV, i.e. the dynamics of electrons above this energy is revealed. Note that the F I(3p $^2P^0_{3/2}$) can be created through cascade processes from upper levels based on the NIST database [28], but its contribution to the total measured intensity is less than 15% and can be neglected in this experiment. Additionally, we have verified that there is only one line at 703.74 nm within the filter measurement range emitting from our plasma by employing a high-resolution Echelle ESA 4000 spectrometer (resolution around 0.02 nm at 700 nm). Further detailed information about the diagnostic can be found elsewhere [29–31].

2.2. Computational method

The computational part of this study is based on a one-dimensional in space and three-dimensional in velocity (1d3v) particle in cell simulation complemented with a Monte Carlo treatment of collision processes (PIC/MCC). The particles traced in the simulations are electrons, as well as CF_3^+, CF_2^+, CF_3^- and F^- ions. The cross sections for the collision process of electrons with the neutral gas are adopted from Kurihara *et al* [32], with the exception of the electron attachment processes that produce CF_3^- and F^-, for which the cross sections are adopted from Bonham [33]. Figure 2 shows the cross sections of the electron reactions included in the simulation. The cross section of the electron impact excitation process that leads to the excitation of F atoms from the ground state to the 3p $^2P^0_{3/2}$ level (for which the excitation rate is measured in the experiment by PROES) is also displayed. Note, that this excitation is traced in the simulation, but it does not change the dynamics of the electrons as it is not an important reaction in CF_4 discharges, but is only used for diagnostic purposes here.

The reactions between the various ions and the neutral gas included in the model are the same as those used in [34] and are included by using an ion-molecule collision model for endothermic reactions [35, 36]. Details can be found in our previous work [37].

The recombination processes between positive and negative species and their rate coefficients are listed in table 1. The rate coefficients of electron-positive ion recombination and ion-ion recombination originate from [36]. We assume that the rate coefficients for the CF_2^+ ions are the same as for the CF_3^+ ions.

In the simulation, the same discharge conditions are used as in the experiment, i.e. a pressure of 20 Pa, an electrode gap of 2.5 cm and a frequency of 13.56 MHz. We assume a gas temperature of 320 K. To simulate the process of voltage increase and decrease as implemented in the experiment, each simulation run is initialized with the converged result at the previous value of the voltage, i.e. the simulation at a given voltage is either started based on a converged simulation at lower or higher voltage. For the interactions of the charged particles with the electrode surfaces, we include elastic reflection of the

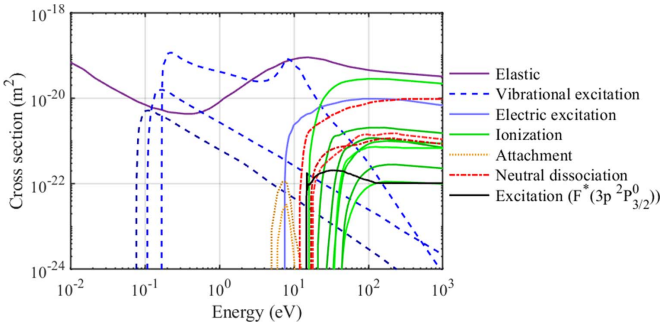

Figure 2. Cross sections of e-CF_4 collisions included in the simulation.

Table 1. Recombination processes considered in the simulation.

Reaction	Rate coefficient (m^3s^{-1})
$CF_3^+ + e^-$	$3.95\times10^{-15}T_i^{-1}T_e^{-0.5}$
$CF_3^+ + F^-$	1×10^{-13}
$CF_3^+ + CF_3^-$	1×10^{-13}
$CF_2^+ + e^-$	$3.95\times10^{-15}T_i^{-1}T_e^{-0.5}$
$CF_2^+ + F^-$	1×10^{-13}
$CF_2^+ + CF_3^-$	1×10^{-13}

electrons and secondary electron emission by positive ions. Electrons are reflected at the electrodes with a probability of 0.7. This value is adapted from a multi-diagnostic experimental validation study performed in a similar reactor as the one used in this work in argon gas [30]. In the CF_4 discharge studied here, no significant deposition on the electrodes was observed in the experiments, thus we assume 0.7 to be a realistic value. Ion induced secondary electron emission is switched on and off in the simulation to study its effect on the hysteresis. The corresponding emission coefficient (γ) is varied from 0 to 0.15.

The simulation code is based on an explicit scheme. It comprises 1200 spatial grid points and uses 8000 integration time steps within an RF period. The simulation settings fulfill all stability criteria and the code has been validated experimentally before [37].

Based on the PIC/MCC simulation results for the F atom generation rate $S_F(x)$, the axial density profile of F atoms, $n_F(x)$, is determined by solving the stationary diffusion equation:

$$-D\frac{\partial^2 n_F(x)}{\partial x^2} = S_F(x), \tag{1}$$

where $S_F(x)$ is the rate of F atom generation by electron impact dissociative ionization and neutral dissociation of CF_4. D is the diffusion coefficient of F atoms in CF_4 gas calculated based on the Chapman–Enskog theory [38]:

$$D = \frac{1.86\times10^{-3}T^{3/2}\left(1/M_F + 1/M_{CF_4}\right)^{1/2}}{(p/101325)\,\sigma_{12}^2\,\Omega}. \tag{2}$$

Here, T is the gas temperature in Kelvin ($T = 320$ K in this work), p is the pressure in Pascal, M_F and M_{CF_4} are the molecular weights of F and CF_4. The collision diameter $\sigma_{12} = (\sigma_F + \sigma_{CF_4})/2$ is the arithmetic average of the Lennard–Jones collision cross section of the F atoms ($\sigma_F = 2.968$Å) and CF_4 molecules ($\sigma_{CF_4} = 4.662$Å) [39]. The dimensionless quantity, Ω, is determined by the depths of the Lennard–Jones potential wells of F and CF_4 ($\varepsilon_F = 112.6\,\mathrm{K}, \varepsilon_{CF_4} = 134\,\mathrm{K}$) [39].

Previous experimental studies have shown that under the discharge conditions studied in this work, the dominant loss process of F atoms is their reaction with CF_x radicals at boundary surfaces [40, 41]. The loss coefficient (including reaction and recombination probabilities) of F atoms at stainless steel surfaces is $\alpha_{loss} = 0.02$ [42]. The following boundary condition of the third kind is used for solving the diffusion equation for $n_F(x)$:

$$\frac{n_F(x = 0/L)}{\kappa} = \left|\frac{\partial n_F}{\partial x}\right|_{x=0/L}, \tag{3}$$

where $\kappa = l(2 - \alpha_{loss})/(\sqrt{3}\alpha_{loss})$. l is the collisional mean free path of F atoms in CF_4 gas, which is calculated from the diffusion coefficient using [43]:

$$l = \frac{4}{\sqrt{3\pi}}\left(\frac{m}{3k_B T_g}\right)^{1/2} D. \tag{4}$$

Based on the diffusion coefficient and this boundary condition, equation (1) can be solved to obtain the time-averaged axial F atom density distribution, which is relevant for a variety of plasma processes [4, 44]. Note that the F atom density is not considered as part of the background gas in the simulation due to its relatively low density compared to CF_4 at the present conditions. The F atom density is calculated separately based on the PIC/MCC simulation after its convergence by taking the generation rate of F atoms from the PIC/MCC simulation as input parameter for the diffusion equation.

3. Results

Below, we present our experimental and computational results. All these were obtained at a CF_4 pressure of 20 Pa, at 2.5 cm electrode separation and a driving frequency of 13.56 MHz. Most of the simulation results are shown for a secondary electron yield of $\gamma = 0.07$ as this provides the best agreement with the experimental results. At the end of the section, the effects of different γ-coefficients on the hysteresis will, however, be discussed.

Figure 3 shows the variation of the electron impact excitation rate from the F atom ground state into the $3p\ ^2P^0_{3/2}$ level as a function of the driving voltage amplitude, for increasing and decreasing voltage, as obtained from PROES measurements (a) and PIC/MCC simulations (b) by space and time averaging over the region of interest (ROI) which is marked by a white rectangle in figures 4(a1) and 5(a1). This ROI in the experimentally and computationally obtained spatio-temporally resolved plots of this excitation rate is selected in a way that it covers parts of the bulk region and the time of maximum current within the RF period. Thus, strong excitation in this ROI indicates the presence of a strong bulk electric field and the presence of the DA mode. The experimental data shown in figure 3(a) clearly show a hysteresis, i.e. increasing the driving voltage amplitude from a low initial value leads to a decrease of the excitation rate, up to about 285 V. However, decreasing the voltage starting from a high initial value of 285 V does not result in the same excitation rates for a given voltage amplitude. Instead, lower values are observed compared to the results measured at increasing voltage amplitudes. Two steady states of the plasma are observed within a certain voltage range depending on whether the voltage is increased from a low initial value or decreased from a high initial value, resulting in a hysteresis. Under the conditions of this experiment, the voltage range, where this hysteresis occurs, is about 210–290 V. In the simulation, a similar phenomenon is observed as shown in figure 3(b), and the voltage range of the hysteresis is 210–260 V for a γ-coefficient of 0.07. Compared to the experimental results, in the simulation, the voltage range, where the hysteresis occurs, and the exact shape of the hysteresis loop are slightly different. This can be a result of the simplified one-dimensional (1D) approach of the simulation, while the experiment is more complex. The simplified treatment of plasma-surface interactions in the simulation might also play a role. Nevertheless, despite the simplicity of the simulation, the main physical effect, i.e. the presence of a hysteresis loop, is well reproduced and occurs in a similar voltage range as compared to the experiment.

Figure 4 shows the spatio-temporal distribution of the electron impact excitation rate measured by PROES for different driving voltage amplitudes. The first row, from left to right, displays the results obtained by increasing the voltage from a low initial value, while the second row, from right to left, presents the corresponding results when the voltage is decreased from a high initial value. The symmetrical excitation rate distribution indicates the good geometric symmetry of the experimental setup. In figure 4(a1) at 210 V, maximum excitation occurs at both electrodes during the local sheath expansion phase. The excitation maximum is not restricted to the vicinity of the sheath edge, but it extends into the plasma bulk region. This is caused by the presence of a significant bulk electric field at these times of high RF current within the RF period [14] indicating that the plasma operates in a hybrid α-/DA-mode. As the voltage is increased to 255 V, the excitation in the plasma bulk and, thus, the DA-mode are reduced, while the α-mode becomes more pronounced. Subsequently, at 287 V, the discharge undergoes a transition into pure α-mode. When the voltage is gradually decreased from a high initial value, such as 287 V as depicted in figure 4(b3), the DA-mode is significantly less pronounced at 255 V as compared to the situation observed at the same voltage, when the voltage was increased (see figure 4(a2)). This result shows that the plasma is operated in a different steady state at 255 V depending on whether the voltage is increased or decreased with a larger region of electron impact excitation rate in the voltage increasing branch. The reverse mode transition into a hybrid

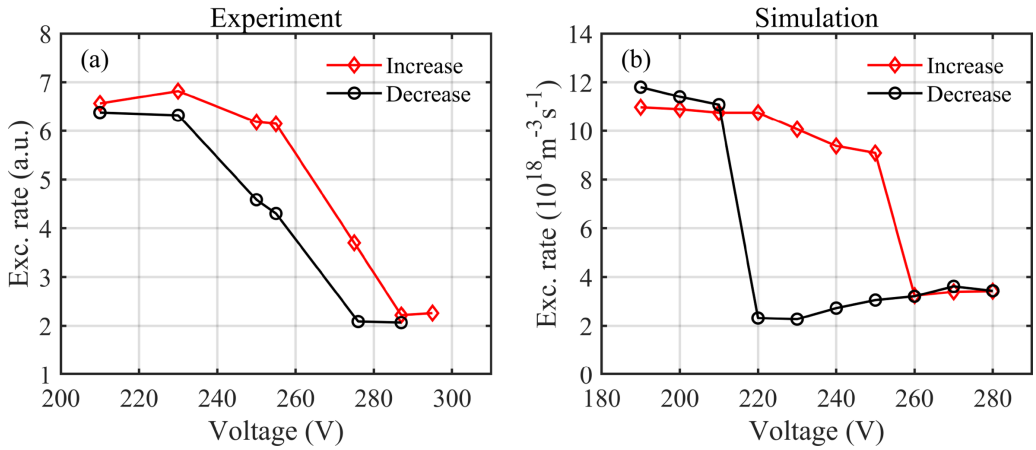

Figure 3. Electron impact excitation rate from the F atom ground state into the 3p $^2P^0_{3/2}$ level as a function of the driving voltage amplitude, for increasing and decreasing voltage. (a) Space- and time-averaged measured PROES data averaged over the region of interest marked in figure 4(a1). (b) Space- and time-averaged simulation results averaged over the region of interest marked in figure 5(a1). Discharge conditions: CF_4, 13.56 MHz, 20 Pa, 2.5 cm electrode gap.

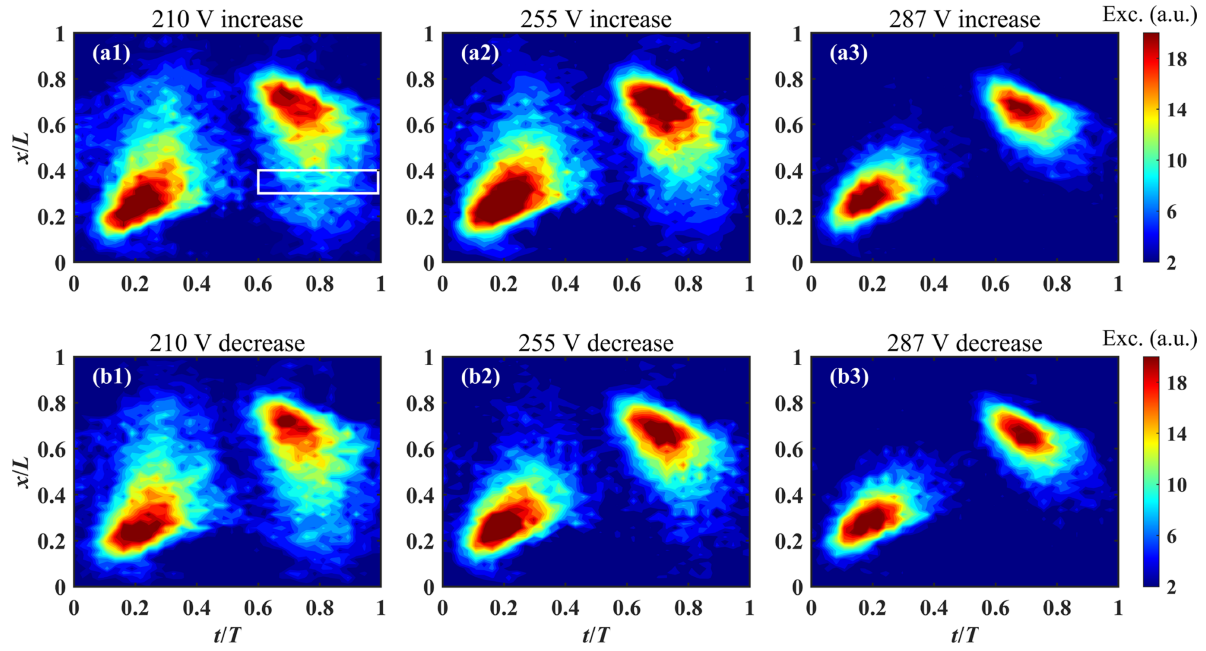

Figure 4. Spatio-temporal distributions of the electron impact excitation rate from the F atom ground state into the 3p $^2P^0_{3/2}$ level measured by PROES for an increasing (a1)–(a3) and a decreasing (b1)–(b3) driving voltage amplitude. The white rectangle in (a1) indicates the region of interest which is used to obtain the excitation rate shown in figure 3(a) by space and time averaging over this region. The discharge conditions are the same as those shown in figure 3.

α-/DA-mode with significant excitation in the plasma bulk is only observed at 210 V. A similar behavior of this spatio-temporally resolved excitation rate is observed computationally for increasing and decreasing voltage amplitude as shown in figure 5. In fact, a more significant difference between the results obtained at 230 V for increasing and decreasing voltage amplitude is identified in the compational results as compared to the experimental findings (see figures 5(a2) and (b2)). Clearly a hysteresis is found. These differences between experimental and computational results might be caused by the fact that the simulation is a simplified 1D model, while the experiment is more complex. The simplified treatment of plasma-surface interactions in the simulation might also play a role.

Based on the good agreement between experimental and computational results, as shown by figures 3–5, the simulation is believed to provide reliable data for various additional plasma parameters, that cannot be measured easily. In this way, a more detailed fundamental understanding of the hysteresis can be obtained. Figure 6 shows the axial profile of the time averaged electron (a, c) and CF_3^+ ion (b, d) density at three selected voltage amplitudes in the upper (increasing voltage) (a, b) and lower hysteresis branch (decreasing voltage) (c, d) obtained from the simulation. For the increasing

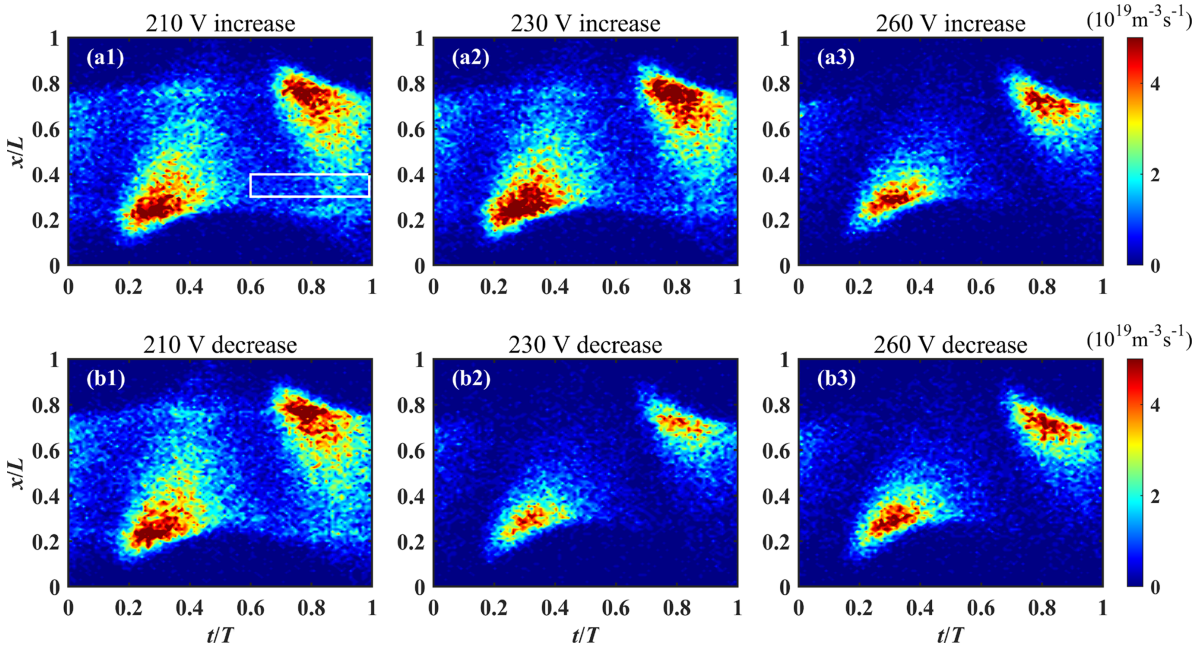

Figure 5. Spatio-temporal distributions of the electron impact excitation rate from the F atom ground state into the 3p $^2P^0_{3/2}$ level obtained from the PIC/MCC simulation for an increasing (a1)–(a3) and a decreasing (b1)–(b3) driving voltage amplitude. The white rectangle in (a1) indicates the region of interest which is used to obtain the excitation rate shown in figure 3(b) by space and time averaging over this region. The discharge conditions are the same as those shown in figure 3.

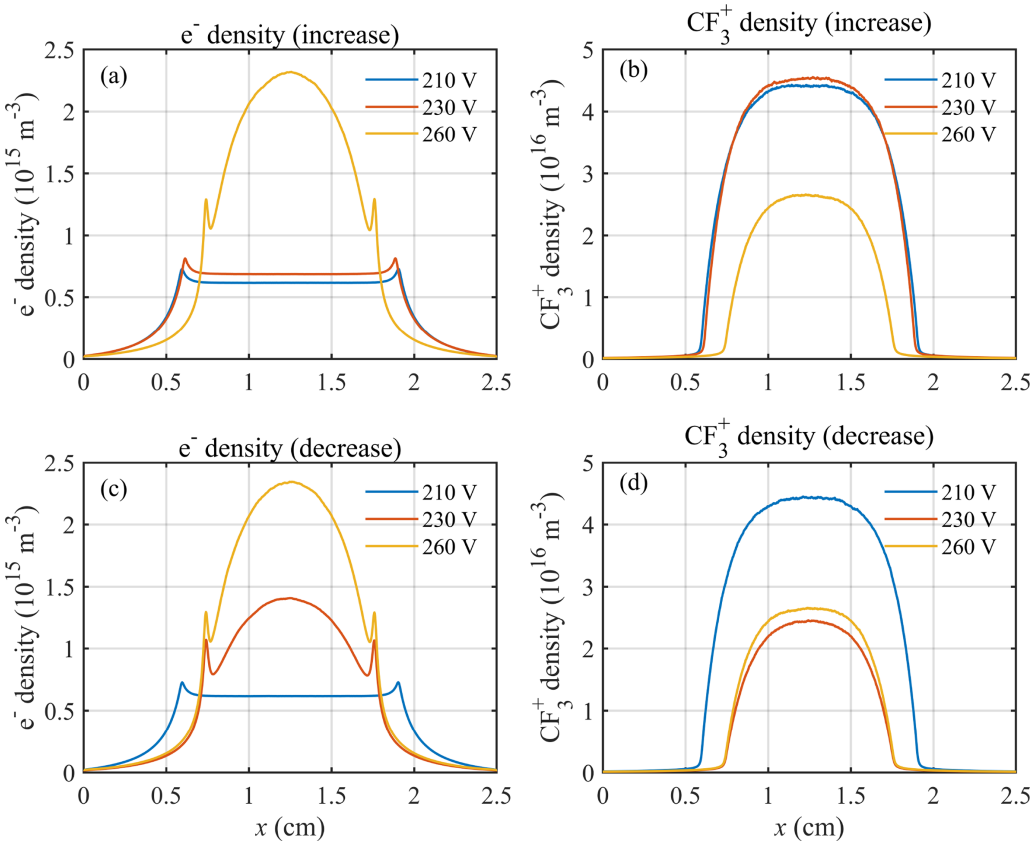

Figure 6. Computationally obtained axial profiles of the time averaged electron (a), (c) and CF_3^+ (b), (d) ion density at different driving voltage amplitudes as the voltage increases in the upper hysteresis branch (a), (b) and decreases in the lower hysteresis branch (c), (d). The discharge conditions are the same as those shown in figure 3.

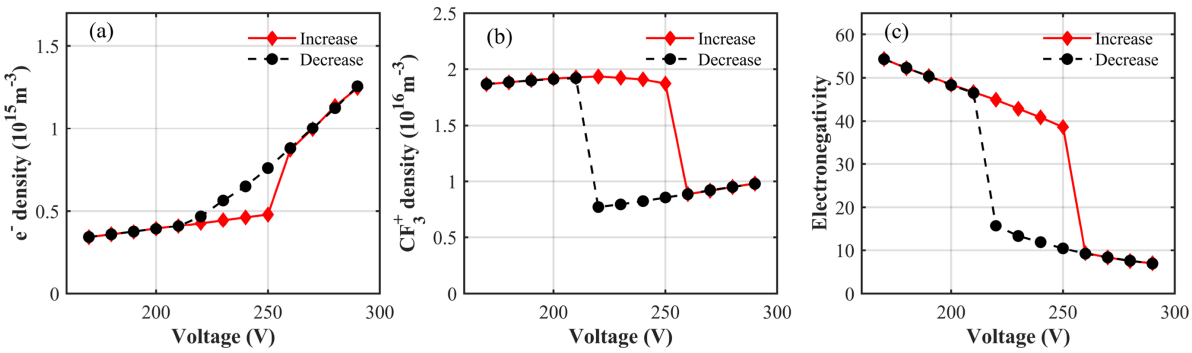

Figure 7. Computationally obtained spatially and temporally averaged electron density (a), CF_3^+ ion density (b) and electronegativity (c) as a function of the driving voltage amplitude for the upper (increasing voltage) and lower (decreasing voltage) hysteresis branches. The discharge conditions are the same as those shown in figure 3.

voltage branch, at 210 V, the electron density in figure 6(a) exhibits two peaks at the two sheath boundaries, which is a typical characteristic of the electron density profile in electronegative plasmas [15]. The CF_3^+ density is higher than the electron density in the bulk region as shown in figure 6(b), where quasi-neutrality is maintained by the presence of negative ions. At a higher voltage of 230 V, the electron and CF_3^+ ion density increase slightly. Continuing to increase the voltage to 260 V, there is a significant change of the charged particle densities caused by the transition of the discharge mode mentioned earlier. The electron density in the bulk region increases strongly, while the CF_3^+ ion density decreases significantly and the width of the plasma bulk is decreased. These changes of the charged particle densities lead to a change of the electronegativity, which is much lower at 260 V compared to 230 V.

For the decreasing voltage branch, the electron and CF_3^+ ion density profiles at 260 V and 210 V are essentially the same as those observed in the increasing voltage branch at the same driving voltage amplitudes. However, at 230 V, the charged particle density profiles differ between the upper and lower branches of the hysteresis loop. In the lower branch, for decreasing voltage, the CF_3^+ ion density is lower and the electron density is higher in the plasma bulk compared to the upper branch, for increasing voltage. Apparently, there are substantial differences in electron and ion densities between the two steady states of the plasma observed at 230 V in the simulation.

Figure 7 shows the variation of the spatially and temporally averaged electron density (a), CF_3^+ ion density (b) and electronegativity (c) with increasing and decreasing voltage based on simulation results. When the voltage increases, the electron density initially increases only slightly, followed by a sudden jump to a high value, before gradually increasing at a slower rate. However, with the gradual decrease in voltage from an initial high value, the electron density decreases gradually without abrupt changes, thereby leading to the formation of a hysteresis loop. The space and time averaged CF_3^+ ion density, shown in figure 7(b) jumps to a lower density at a higher voltage in the upper hysteresis branch, i.e. for increasing voltage, while it jumps back to the high density at a lower voltage in the lower hysteresis branch, i.e. for decreasing voltage. The variation of the F^- ion density with voltage exhibits a similar hysteresis loop compared to that of the CF_3^+ ion density. The electronegativity also displays a hysteresis loop as shown in figure 7(c). Note that the plasma is electronegative throughout the entire voltage range, even during the transition to the α-mode at high voltages, but the electronegativity changes significantly and differently along the upper vs. the lower hysteresis branches.

Further insight into the physical mechanisms of the hysteresis can be gained based on additional simulation results. Figure 8 shows the spatio-temporally resolved mean electron energy at different voltages within the two hysteresis branches based on simulation results. In the increasing voltage branch, when the voltage is 210 V, the plasma operates in the DA-/α-hybrid mode. As depicted in figure 8(a1), high-energy electrons with energies exceeding 5 eV are present in the entire plasma bulk region, resulting in an efficient generation of negative ions via electron attachment, whose cross section is high at electron energies above a threshold of about 4 eV (see figures 2 and 9(a1)). When the voltage increases to 230 V, due to a weak increase in electron density and the corresponding increase of the plasma conductivity as well as the decrease of the drift electric field in the bulk, the electron energy slightly decreases, but its distribution is very similar to the one observed at 210 V, i.e. the mean electron energy is still high in the bulk. Correspondingly, the electron attachment rate increases slightly due to the increased electron density. The high mean electron energy in the plasma bulk region is caused by the electron acceleration by the expanding sheaths and the high DA electric field in the bulk. Figure 10(a) depicts the spatio-temporal distribution of the electric field at 230 V in the upper hysteresis branch (increasing voltage), where the high bulk electric field is caused by the low conductivity resulting from the reduced electron density in this strongly electronegative discharge (see figure 7(c)). This high bulk electric field results in a large number of electrons surpassing the energy threshold required for electron attachment, leading to a strong generation of negative ions. This process maintains a low electron density, consequently sustaining the high electronegativity and bulk electric field, forming a positive feedback mechanism. The feedback mechanism persists until the driving voltage amplitude reaches 260 V. At this voltage,

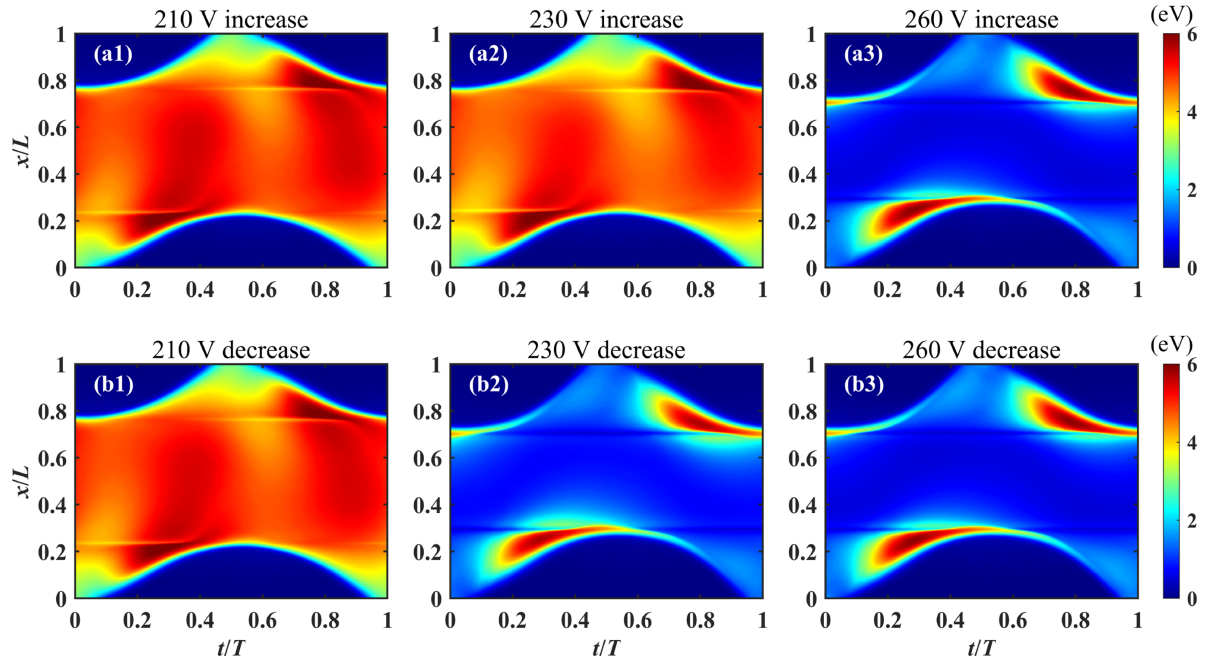

Figure 8. Computationally obtained spatio-temporal distribution of the mean electron energy for the upper (increasing voltage, (a1)–(a3)) and lower (decreasing voltage. (b1)–(b3)) hysteresis branches. The discharge conditions are the same as those shown in figure 3.

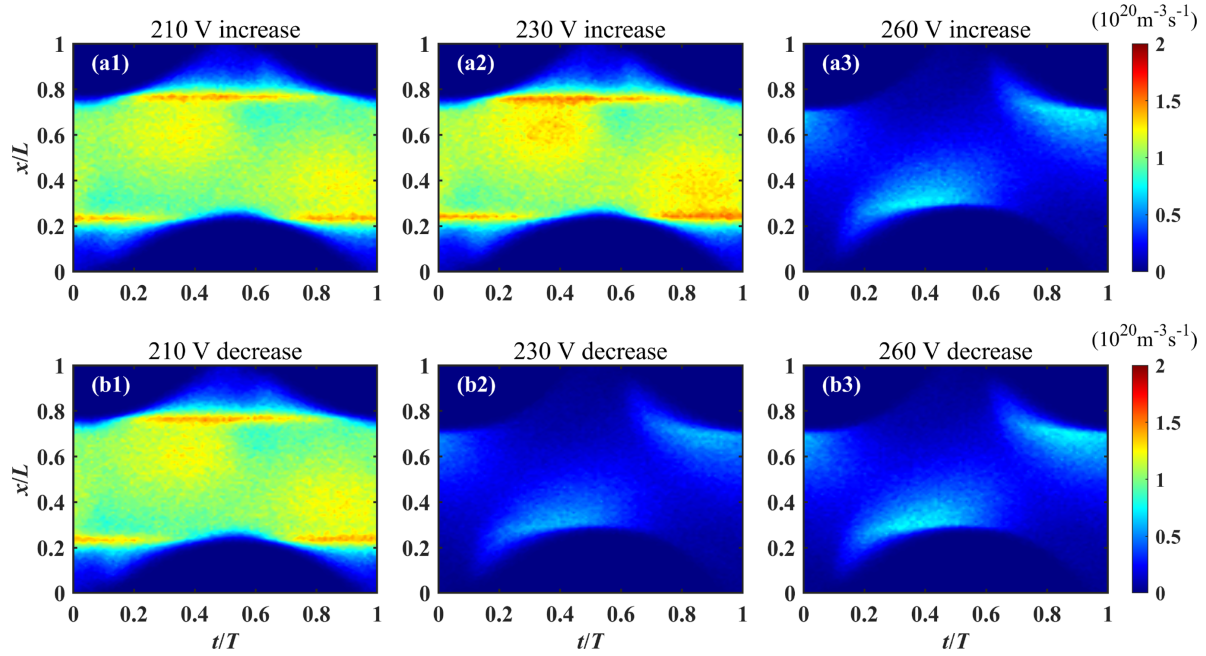

Figure 9. Computationally obtained spatio-temporal distribution of the electron attachment rate that results in the generation of F^- ions for the upper (increasing voltage, (a1)–(a3)) and lower (decreasing voltage. (b1)–(b3)) hysteresis branches. The discharge conditions are the same as those shown in figure 3.

the increase in electron density breaks the feedback loop by enhancing the plasma conductivity and reducing the bulk electric field to values that are insufficient to accelerate a high number of electrons to energies that are high enough to form negative ions by electron attachment, as shown in figures 8(a3) and 9(a3). Consequently, the discharge transits to the α-mode and the electron density suddenly increases while the F^- ion density decreases.

In the lower hysteresis branch, the voltage is decreased from a value of 260 V at which the plasma operates in the α-mode characterized by a high electron density and conductivity. The bulk electric field is, therefore, low. High-energy electrons are predominantly present near the edges of the expanding sheaths, which causes the electron attachment rate to be high only at the expanding sheath edges, but to be low in the bulk, as shown in figures 8(b3) and 9(b3). Decreasing the

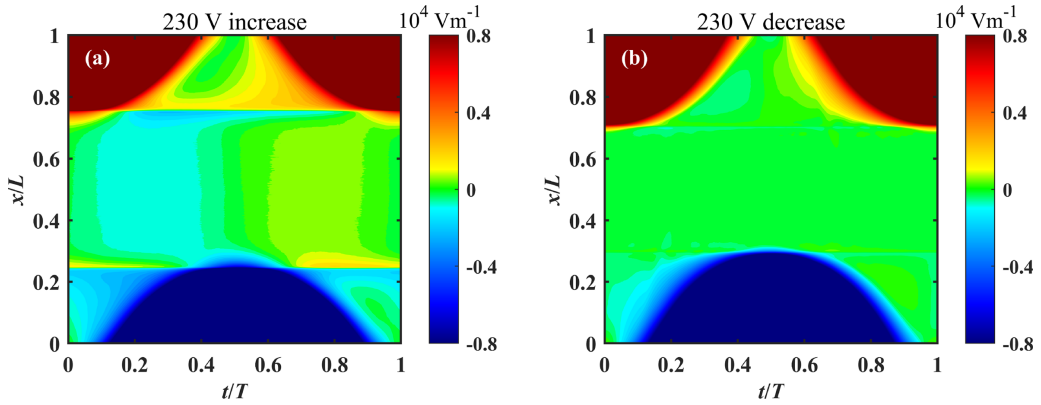

Figure 10. Computationally obtained spatio-temporal plots of the electric field at two steady states of the plasma at 230 V in the upper (increasing voltage, (a)) and lower (decreasing voltage, (b)) hysteresis branches. The discharge conditions are the same as those shown in figure 3.

voltage to 230 V, the high electron density at the original discharge conditions at 260 V is maintained. Due to the high electron density the bulk electric field is low, as shown in figure 10(b). Consequently, the mean electron energy remains low in the bulk and its spatio-temporal distribution is similar to the one observed at the original higher voltage, in strong contrast to the spatio-temporal distribution of the mean electron energy at 230 V in the upper hysteresis branch for increasing voltage. Thus, in the lower hysteresis branch (decreasing voltage), the electron attachment rate remains low in the plasma bulk (see figure 9(b2)). Clearly, this steady state of the discharge observed in the lower hysteresis branch is markedly different from the state observed in the upper hysteresis branch for increasing voltage, although the driving voltage amplitude and all other external control parameters are identical. The presence of these two steady states is caused by the different previous plasma states present at the higher or lower voltages. As the voltage is further reduced, the electron density continues to decrease. When the voltage reaches 210 V, the electron density becomes so low that the conductivity is reduced and the bulk electric field is increased to an extent that electrons are accelerated to high enough energies in the plasma bulk to cause strong electron attachment, which results in a strong production of negative ions. This reduces the electron density and conductivity even more and ultimately results in the operation of the discharge in a hybrid α-/DA-mode and a closure of the hysteresis loop, i.e. only a single steady state of the plasma is observed at this voltage, both for increasing and decreasing voltage.

The presence of this hysteresis effect has strong consequences on the electron energy distribution function (EEDF) and, thus, on the production of neutral radicals and positive ions via electron impact dissociation and ionisation of the background gas. It is, therefore, expected to be relevant for applications such as dielectric plasma etching, where the flux of F atoms to the wafer plays an important role for the etch rate. Figure 11 shows the normalized EEDFs obtained from the simulation and averaged over 10% of the electrode gap in the discharge center at two different voltages of 230 V and

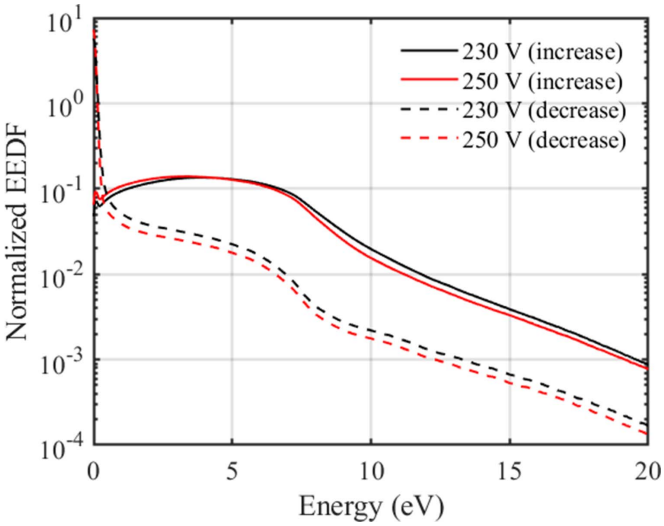

Figure 11. Computationally obtained time averaged EEDF in the discharge center (spatially averaged over 10% of the electrode gap in the center) in the upper and lower branches of the hysteresis loop, i.e. for increasing and decreasing driving voltage amplitude, at 230 V and 250 V. The discharge conditions are the same as those shown in figure 3.

250 V in the upper and lower branches of the hysteresis loop, i.e. for increasing and decreasing voltage, respectively. The difference between the two plasma states present in the different hysteresis branches for identical discharge conditions is evident. In the upper branch (increasing voltage), a much higher number of high-energy electrons is generated compared to that in the lower branch (decreasing voltage) due to the different bulk electric fields.

The different EEDFs in the upper and lower branches of the hysteresis loop affect the production of F atoms by dissociative ionization and electron impact dissociation of the background gas as well as the production of ions due to the dependence of the corresponding cross sections on the electron energy as well as due to the different electron densities. The different EEDFs present in the two hysteresis branches under

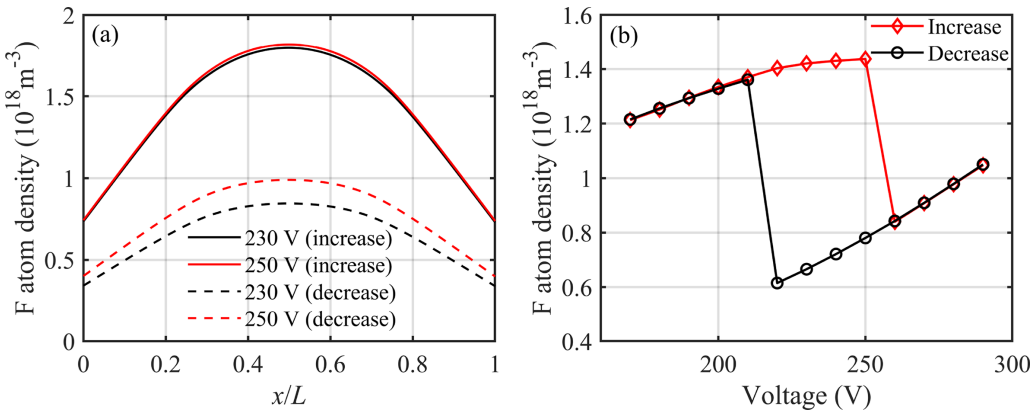

Figure 12. Computationally obtained axial profiles of the F atom density at 230 V and 250 V for both hysteresis branches (a) and space- and time-averaged F atom density as a function of the driving voltage amplitude in both hysteresis branches, i.e. for increasing and decreasing voltage (b). The discharge conditions are the same as those shown in figure 3.

identical conditions lead to different densities of F atoms. Based on the stationary diffusion model introduced in the computational method section, the F atom density is calculated as shown in figure 12. Panel (a) illustrates the axial distribution at two different voltages obtained in the two hysteresis branches, respectively, and panel (b) shows the variation of the space averaged F atom density as a function of the driving voltage amplitude for increasing and decreasing voltage. According to the reaction cross sections shown in figure 2, the major production process of F atoms in CF_4 plasmas is electron impact dissociative ionization ($CF_4 + e \rightarrow CF_3^+ + F + 2e$). Due to the higher electric field in the bulk region in the upper hysteresis branch, i.e. for increasing voltage, more high-energy electrons are generated, resulting in an enhancement of the generation rate of F atoms. Compared to the lower hysteresis branch (decreasing voltage), the F atom density is higher in the discharge center by about 80% in the upper hysteresis branch, as shown in figure 12(a). As depicted in figure 12(b), a similar hysteresis of the spatially averaged F atom density is observed, too. These results show that operating the discharge in the upper hysteresis branch might be beneficial for etching applications due to the higher F atom density under otherwise identical discharge conditions. Practically this means that the plasma should be generated initially at a lower voltage and then the voltage should be increased rather than generating the discharge initially at a higher voltage and then decreasing it.

The flux-energy distribution of positive ions at the electrodes also plays an important role in plasma processes, such as ion implantation where it can change material surface properties. Controlled energetic ion bombardment can enhance the etch rate and can promote chemical vapor deposition processes to improve film quality and uniformity. In these processes, uniform, well-controlled and stable ion fluxes and ion energies are necessary to ensure high process stability and yield. However, the presence of the hysteresis can induce process instabilities, since it leads to two plasma steady states under the same discharge conditions. As shown in figure 13, the ion flux (panel (a)) and the mean ion energy (panel (b)) at the powered electrode are higher in the upper hysteresis branch, when the voltage is increased. Within the voltage range of the hysteresis loop, the previous state of the plasma affects the ion flux and energy. For the same driving voltage amplitude, there is a difference of nearly 50% in the ion flux between the two plasma steady-states, while the difference in the mean ion energy is more than 5 eV. A small change in voltage near the value at which the discharge mode changes can cause these differences in ion flux and ion energy.

In previous works, hysteresis effects were observed in electropositive discharges and explained by a mode transition between a 'volume dominated' (VD) regime and an 'active sheath' (AS) regime [23, 24]. The VD regime is characterized by a relatively low plasma density and high electron energy, today known as α-mode, while in the AS regime, the electron energy profile exhibits two maxima in the sheaths, today known as the γ-mode. Thus, in contrast to this work, the previously observed hysteresis was caused by an α- to γ-mode transition, while it is caused by a DA- to α-mode transition in this work. In the γ-mode, ion induced secondary electrons play a crucial role, whose emission probability depends on the electrode material. As such γ-electrons were previously observed to affect hysteresis effects, we will investigate their effects on the hysteresis in CF_4 discharges in the following. Figure 14 shows the effects of different γ-coefficients on the hysteresis of the spatially and temporally averaged electron (the first row) and CF_3^+ ion (the second row) density based on simulation results. Similar hysteresis loops are observed for different γ-coefficients. Even if γ is set to 0, the hysteresis still persists, indicating that its presence is not caused by secondary electrons. This means that the hysteresis effects observed in this study and previous findings are caused by different mechanisms, i.e. different mode transitions of the plasma, although secondary electron emission also influences the effect observed in our study. As the γ-coefficient is increased, the electron and CF_3^+ density increase slightly and the voltage range, where the hysteresis loop occurs, moves towards lower voltages. This is caused by the fact that at a given driving voltage amplitude more secondary electron emission leads to higher electron densities and

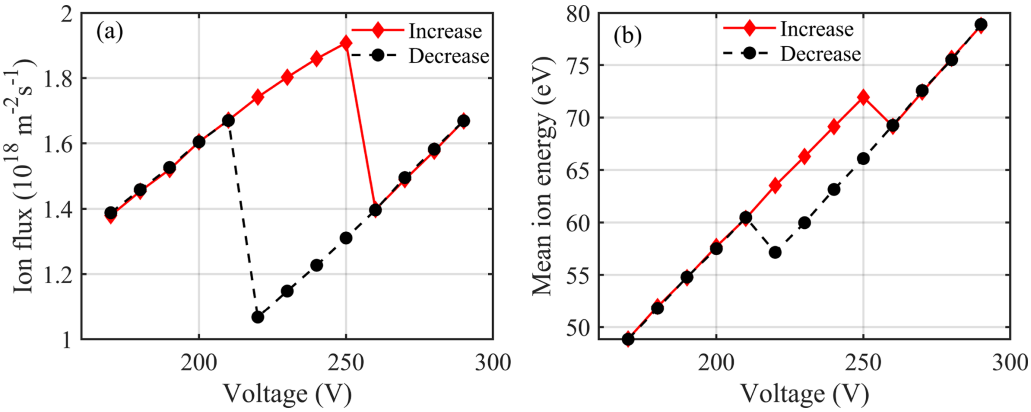

Figure 13. Computed CF_3^+ ion flux (a) and mean ion energy (b) at the powered electrode as a function of the driving voltage amplitude for increasing and decreasing voltage. The discharge conditions are the same as those shown in figure 3.

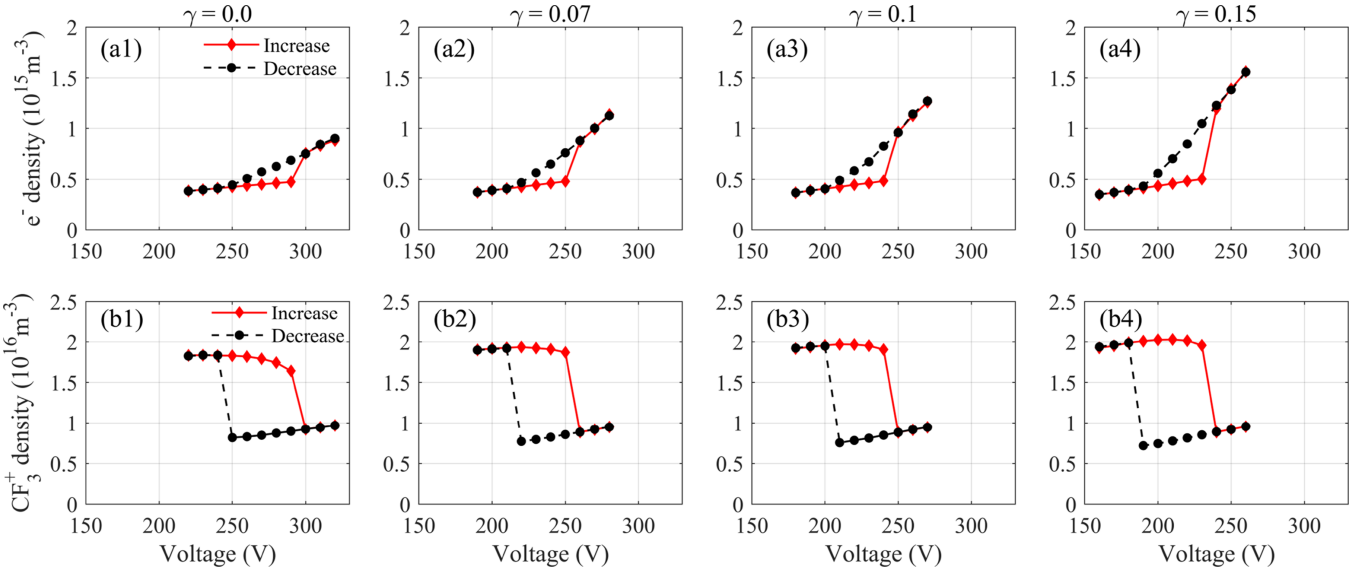

Figure 14. Computed electron (first row) and CF_3^+ ion (second row) density as a function of the driving voltage amplitude for increasing and decreasing voltage and for different ion induced secondary electron emission coefficients (γ). The discharge conditions are the same as those shown in figure 3.

plasma conductivity, which leads to a lower bulk electric field, lower mean electron energies in the bulk and less negative ion formation. This causes the discharge mode transition from the DA- to the α-mode to occur at a lower voltage.

4. Conclusions

A hysteresis induced by changing the driving voltage amplitude in capacitively coupled CF_4 plasmas was observed and studied experimentally by PROES and PIC/MCC simulations. Based on this experimental validation, the physical mechanism behind the observed hysteresis was clarified by the simulation results.

The hysteresis was found to be caused by a mode transition of the plasma between a hybrid DA-/α-mode and a pure α-mode induced by changing the driving voltage amplitude. This mode transition occurs at different voltage amplitudes depending on whether the voltage is increased or decreased. In case of increasing voltage, the plasma initially operates in a hybrid DA-/α-mode at low voltage. The electron density and the plasma conductivity are low, causing a high electric field in the plasma bulk region. Many electrons are accelerated to high enough energies (above 4 eV) to cause dissociative attachment to generate negative ions. For moderate increases of the voltage, the fact that the discharge was previously operated at lower voltage keeps the discharge in its original mode due to a positive feedback mechanism, as the production of negative ions consumes electrons, preventing the increase of the electron density and plasma conductivity. However, when the voltage reaches higher values, the electron density and, thus, the conductivity increase significantly. Consequently, the energy of electrons in the bulk region decreases and is no longer high enough to produce negative ions by electron attachment efficiently. As a result, the feedback mechanism is broken, the electron density increases strongly and a discharge mode transition to a pure α-mode occurs.

If the driving voltage amplitude is decreased from an initially high value, the reverse mode transition from the α- to the hybrid DA-/α-mode occurs at lower voltages compared to the mode transition point observed for increasing voltage. In the plasma bulk region, the electron density is now initially high, the bulk electric field is weak and the mean electron energy is low. As the voltage decreases, the electron density decreases gradually, but remains high even for moderately decreased voltages, since the discharge was previously operated at higher voltage with high electron densities. Therefore, two different steady states of the plasma are generated for distinct driving voltage amplitudes, i.e. a hysteresis is formed. As the voltage continues to decrease, the electron density decreases to a point where the plasma conductivity is low enough and the bulk electric field is high enough to accelerate electrons to high enough energies to cause a strong formation of negative ions via electron attachment. This leads to a discharge mode transition into a hybrid DA-/α-mode and marks the end of the hysteresis loop.

In the two steady states of the plasma observed for identical driving voltage amplitudes, there is a significant difference in the EEDF, leading to a higher F atom density in the voltage increasing branch. The ion flux and energy at the electrodes, which are additional application relevant plasma parameters, are also higher in the voltage increasing branch.

Different from hysteresis effects found previously in electropositive discharges, the presence of the hysteresis loop observed in this work is not related to secondary electrons, i.e. the physical origin of its generation is different. But the choice of the γ-coefficient (different electrode materials) affects the voltage range where the hysteresis occurs in this work. As the γ coefficient increases, the hysteresis loop shifts towards lower voltage.

Data availability statement

All data that support the findings of this study are included within the article (and any supplementary files).

Acknowledgments

This work has been financially supported by the National Natural Science Foundation of China (NSFC) (Grant Nos. 12275043 and 12020101005), China Scholarship Council (No. 202106060085), the Hungarian National Office for Research, Development, and Innovation (NKFIH) via the Grant K134462, and the German Research Foundation via Project 138690629.

ORCID iDs

Xiao-Kun Wang https://orcid.org/0000-0003-4160-5316
Ihor Korolov https://orcid.org/0000-0003-2384-1243
Sebastian Wilczek https://orcid.org/0000-0003-0583-4613
Ranna Masheyeva https://orcid.org/0000-0002-6950-662X
Yong-Xin Liu https://orcid.org/0000-0002-6506-7148
Yuan-Hong Song https://orcid.org/0000-0001-5712-9241
Peter Hartmann https://orcid.org/0000-0003-3572-1310
Zoltán Donkó https://orcid.org/0000-0003-1369-6150
Julian Schulze https://orcid.org/0000-0001-7929-5734

References

[1] Lieberman M A and Lichtenberg A J 2005 *Principles of Plasma Discharges and Materials Processing* (Wiley)
[2] Chabert P and Braithwaite N 2011 *Physics of Radio-Frequency Plasmas* (Cambridge University Press)
[3] Makabe T and Petrovic Z L 2006 *Plasma Electronics: Applications in Microelectronic Device Fabrication* (CRC Press)
[4] Williams P F 2013 *Plasma Processing of Semiconductors* vol 336 (Springer Science & Business Media)
[5] Donnelly V M and Kornblit A 2013 *J. Vac. Sci. Technol.* A **31** 050825
[6] Balachova O, Alves M, Swart J, Braga E and Cescato L 2000 *Microelectron. J.* **31** 213–5
[7] Wilczek S, Schulze J, Brinkmann R P, Donkó Z, Trieschmann J and Mussenbrock T 2020 *J. Appl. Phys.* **127** 181101
[8] Belenguer P and Boeuf J P 1990 *Phys. Rev.* A **41** 4447–59
[9] Schulze J, Heil B G, Luggenholscher D and Czarnetzki U 2008 *IEEE Trans. Plasma Sci.* **36** 1400–1
[10] Proshina O V, Rakhimova T V, Rakhimov A T and Voloshin D G 2010 *Plasma Sources Sci. Technol.* **19** 065013
[11] Kawamura E, Lieberman M A and Lichtenberg A J 2006 *Phys. Plasmas* **13** 053506
[12] Vender D and Boswell R W 1992 *J. Vac. Sci. Technol.* A **10** 1331–8
[13] Daksha M, Derzsi A, Mujahid Z, Schulenberg D, Berger B, Donkó Z and Schulze J 2019 *Plasma Sources Sci. Technol.* **28** 034002
[14] Schulze J, Derzsi A, Dittmann K, Hemke T, Meichsner J and Donkó Z 2011 *Phys. Rev. Lett.* **107** 275001
[15] Derzsi A, Schüngel E, Donkó Z and Schulze J 2015 *Open Chem.* **13** 0044
[16] Liu Y-X, Schüngel E, Korolov I, Donkó Z, Wang Y-N and Schulze J 2016 *Phys. Rev. Lett.* **116** 255002
[17] Schulze J, Donkó Z, Lafleur T, Wilczek S and Brinkmann R P 2018 *Plasma Sources Sci. Technol.* **27** 055010
[18] Phelps A and Petrovic Z L 1999 *Plasma Sources Sci. Technol.* **8** R21
[19] Derzsi A, Bruneau B, Gibson A R, Johnson E, O'Connell D, Gans T, Booth J-P and Donkó Z 2017 *Plasma Sources Sci. Technol.* **26** 034002
[20] Liu G-H, Liu Y-X, Wen D-Q and Wang Y-N 2015 *Plasma Sources Sci. Technol.* **24** 034006
[21] Skarphedinsson G A and Gudmundsson J T 2020 *Plasma Sources Sci. Technol.* **29** 084004
[22] Liu Y-X, Korolov I, Schüngel E, Wang Y-N, Donkó Z and Schulze J 2017 *Phys. Plasmas* **24** 073512
[23] Bohm C and Perrin J 1991 *J. Phys. D: Appl. Phys.* **24** 865
[24] Schweigert I V 2004 *Phys. Rev. Lett.* **92** 155001
[25] Jiang W, Wang H-Y, Zhao S-X and Wang Y-N 2009 *J. Phys. D: Appl. Phys.* **42** 102005
[26] Liu Y-X, Donkó Z, Korolov I, Schüngel E, Wang Y-N and Schulze J 2019 *Plasma Sources Sci. Technol.* **28** 075005
[27] Musielok J, Pawelec E, Griesmann U and Wiese W L 1999 *Phys. Rev.* A **60** 947–55
[28] Kramida A, Yu R and Reader J and NIST ASD Team 2023 (NIST Atomic Spectra Database, National Institute of Standards and Technology) (available: https://physics.nist.gov/asd)

[29] Schulze J, Schüngel E, Donkó Z, Luggenhölscher D and Czarnetzki U 2010 *J. Phys. D: Appl. Phys.* **43** 124016
[30] Schulenberg D A, Korolov I, Donkó Z, Derzsi A and Schulze J 2021 *Plasma Sources Sci. Technol.* **30** 105003
[31] Horváth B, Derzsi A, Schulze J, Korolov I, Hartmann P and Donkó Z 2020 *Plasma Sources Sci. Technol.* **29** 055002
[32] Kurihara M, Petrovic Z L and Makabe T 2000 *J. Phys. D: Appl. Phys.* **33** 2146–53
[33] Bonham R A B 1994 *Jpn. J. Appl. Phys.* **33** 4157–64
[34] Georgieva V 2006 *Computer Modeling of low-Pressure Fluorocarbon-Based Discharges for Etching Purposes PhD Thesis* Universiteit Antwerpen
[35] Nanbu K and Kitatani Y 1995 *J. Phys. D: Appl. Phys.* **28** 324
[36] Georgieva V, Bogaerts A and Gijbels R 2004 *Phys. Rev.* E **69** 026406
[37] Wang X-K, Masheyeva R, Liu Y-X, Hartmann P, Schulze J and Donkó Z 2023 *Plasma Sources Sci. Technol.* **32** 085009
[38] Cussler E L 2009 *Diffusion: Mass Transfer in Fluid Systems* (Cambridge University Press)
[39] Hash D B, Bose D, Rao M V V S, Cruden B A, Meyyappan M and Sharma S P 2001 *J. Appl. Phys.* **90** 2148–57
[40] Sasaki K, Kawai Y, Suzuki C and Kadota K 1997 *J. Appl. Phys.* **82** 5938–43
[41] Tserepi A, Schwarzenbach W, Derouard J and Sadeghi N 1997 *J. Vac. Sci. Technol.* A **15** 3120–6
[42] Kota G P, Coburn J W and Graves D B 1999 *J. Vac. Sci. Technol.* A **17** 282–90
[43] Derzsi A, Hartmann P, Vass M, Horváth B, Gyulai M, Korolov I, Schulze J and Donkó Z 2022 *Plasma Sources Sci. Technol.* **31** 085009
[44] Flamm D L, Donnelly V M and Mucha J A 1981 *J. Appl. Phys.* **52** 3633–9